

# Tectonic Geomorphology and Genetic Analysis Based on Remote Sensing and DEM: A Case Study of the Helanshan Area

Xinru Yang<sup>1</sup>, Weicui Ding<sup>1,\*</sup>, Xuanhua Chen<sup>1</sup>, Lele Han<sup>1</sup>, Daxing Xu<sup>1,2</sup>, Xu Shenglin<sup>1</sup>, Wang Ye<sup>1</sup>

<sup>1</sup>Chinese Academy of Geological Sciences, Beijing, China

<sup>2</sup>School of Earth and Space Sciences, Peking University, Beijing, China

\*Corresponding Author

**Abstract:** Remote sensing interpretation and tectonic geomorphology analysis are crucial for understanding intracontinental tectonic deformation, tectonic evolution, and the coupling relationship between topography and tectonics. The Helanshan fold-thrust belt is situated in the central-western part of the North China Craton, between the Alax block and the Ordos block, representing an intracontinental deformation zone since the Mesozoic. In this paper, remote sensing interpretation, tectonic geomorphology analysis and field geological observation are carried out in the Shizuishan area within the middle segment of the Helanshan fold-thrust belt. The results reveal that the Helanshan region experienced intense intracontinental compressional deformation due to the Yanshanian Orogeny, forming NNE-SSW-trending imbricated thrust-nappe structures, with the mountain uplift manifesting as low elevations in the west and high elevations in the east. From the Oligocene to Miocene, influenced by the north-eastward expansion of the Tibetan Plateau and the subduction and retreat of the Western Pacific Ocean, the Helanshan Eastern Fault reversed, causing in the tectonic subsidence of the Yinchuan Graben and the periodic uplift of the Helanshan, resulting in a geomorphological pattern that is higher in the west and lower in the east.

**Keywords:** Helanshan Fold-Thrust Belt; Remote Sensing Interpretation; Tectonic Geomorphology Analysis; Geomorphological Mechanism

## 1. Introduction

Tectonic geomorphology represents the combined result of internal force (tectonic activity) and external force (erosion) [1,2].

Macroscopic tectonics is the uplift or subsidence of landforms due to plate and crustal activities, and microscopic tectonics is the uplift of mountain ranges and subsidence of basins caused by fold and fracture, and then the present geomorphic patterns are formed by weathering and erosion, which reflects the coupling of the internal and external geologic processes [1-3]. Geomorphic indices quantitatively characterize the surface morphology of tectonically formed landscapes [1-3]. Digital Elevation Models (DEM) and GIS spatial analysis techniques enable the efficient and accurate obtaining of geomorphic indices and quantification of landscape evolution rates, which is one of the effective methods for exploring and revealing the tectonic activities hidden in tectonic landforms [3-5].

Previous studies have shown that the Helanshan and its surrounding regions have entered a stage of strong intracontinental deformation and transformation since the late Paleozoic [6,7]. The collision of the North China Plate with South China caused by the closure of the Paleo-Tethys Ocean, the westward subduction and retreat of the Pacific plate, and the northeastward expansion of the Tibetan Plateau, the Helanshan and its surrounding areas have formed a basin-mountain coupling system with different mechanical properties, complex morphology and intense tectonic deformation [8-15]. Currently, quantitative geomorphological studies of the Helanshan remain scarce, with limited analyses utilizing geomorphic parameters to assess relative crustal movements [16].

Tectonic interpretation based on remote sensing images and the quantitative analysis of tectonic landforms based on DEM can reveal the spatial distribution characteristics of tectonic faults in the study area on a

macroscopic scale, and serve as a fundamental exploration tool to identify areas undergoing tectonic deformation [17-22]. Therefore, this paper integrates Landsat-7 ETM+ image, high-resolution Google Earth image, and ASTER GDEM data, combined with field structural analysis, to analyze the linear fault structure of the Helanshan fold-thrust belt and the geomorphological characteristics of tectonic uplift.

## 2. Regional Setting

The Helanshan tectonic belt represents a significant intracontinental orogenic zone within the North China Block, located at the northeastern edge of the Tibetan Plateau. It is bordered by the Alxa Block to the west, connects with the Hexi Corridor transitional zone to the southwest, and adjoins the stable Ordos Block and Yinchuan Graben to the east (Figure 1b), whose formation was influenced by several tectonic domains [7-23], resulting in complex intracontinental deformation characterized by a series of NNE-trending folds and thrust faults [24] (Figure 1c). Geological studies have shown that the boundary fault between Helanshan and Yinchuan Graben is the Helanshan Eastern Fault, which was a thrust fault in the Late Jurassic and turned into a normal fault from the Cretaceous to the Cenozoic [24-25]. This fault system, along with the Yellow River Fault, the Luhutai Fault, and the Yinchuan Fault, constitutes an intra-graben normal fault system within the Yinchuan Graben [26-29], controlling the Cenozoic sedimentation of Yinchuan Graben [30].

The stratigraphy of the study area is widely exposed, from Precambrian to Cenozoic. The Precambrian mainly includes the Helanshan Group and Qianlishan Group in the Khondalite Belt [6]. The Paleozoic is dominated by the Cambrian, Ordovician, Devonian, Carboniferous, and Permian, and lacks the Silurian. The Triassic strata are mainly the Zhifang Formation and the Yanchang Formation, and their sedimentary environment is a continental fluvial and lacustrine transition system [31], with the Jurassic strata overlying the Upper Triassic in an angularly unconformable contact relationship. The Cretaceous and Cenozoic

deposits are principally distributed within the fault-depression basins on both sides of the Helanshan tectonic belt.

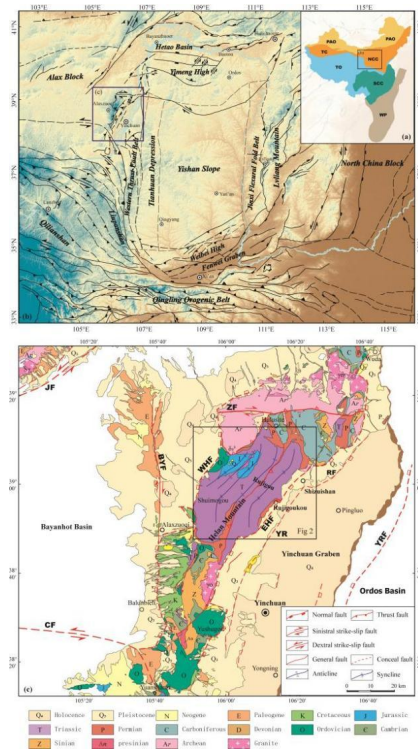


**Figure 1. Helanshan Area Geological Background and Regional Geological Map**

a. China tectonic system: PAO-Palao Asian Ocean tectonic domain; TC-Tarim Craton; NCC-North China Craton; TO-Tethys Ocean tectonic domain; SCC-South China Craton; WP-West Pacific Ocean tectonic domain (modified from [7]); b. Tectonic system of the Ordos and its surroundings (modified from [9-14]); c. Helanshan tectonic belt regional geological map (modified from [14,15]). EHF-Helanshan Eastern Fault; WHF-Helanshan Western Fault; YRF-Yellow River Fault; RF-Rujigou Fault; BYF-Bayanhaote Fault; YF-Yantongshan Fault; QGF - Qingtongxia-Guyuan Fault; CF-Chahan Fault; ZF-Zheng-yiguan Fault; YR-Yinchuan Rift system.

## 3. Data Processing

### 3.1 Data Sources

This study integrates high-resolution Google Earth image, Landsat 7 remote sensing images, and regional 1:200,000 scale geological maps to interpret regional linear fracture structures collectively. The remote sensing identification and interpretation methodology for linear

fracture structures involves processing target images through enhancement techniques to facilitate structural recognition and then extracting the information through manual interpretation. The ASTER GDEM elevation data was jointly developed by the National Aeronautics and Space Administration (NASA) and Japan's Ministry of Economy, Trade and Industry (METI). With a vertical accuracy of 20m and horizontal accuracy of 30m, this high-precision digital elevation model adequately meets the research requirements [16-32].

### 3.2 Remote Sensing Image Data Processing

During visual interpretation of fracture structures, given that the human visual system exhibits significantly better discrimination capability for color than for grayscale, selecting appropriate band combinations is crucial for identifying and interpreting target information. For the Landsat ETM+ image, the panchromatic and multispectral bands are first fused and processed to enhance the spatial resolution to 14.25 m, which is sufficient to delineate geological structural features within the study area [17]. False color synthesis by band 7, band 4, and band 1 can effectively leverage the informational advantages of mid-infrared, near-infrared, and visible bands. This approach enhances image clarity, suppresses noise, and significantly improves the interpretability of geological structures (Figure 2b).

Due to the high correlation among multispectral bands, there is more interfering information, and to address this issue, principal component transformation is applied to maximize data variance through coordinate axis rotation to generate mutually uncorrelated bands [17].

Consequently, principal component analysis (PCA) was performed on six bands (excluding Band 6) of the remote sensing imager, and the first principal component (PC1), containing the highest variance, was utilized for feature identification and extraction, significantly improving the readability and clarity of geological information while reducing spectral reflectance redundancy (Figure 2c). Subsequently, a false color synthesis

was generated using PC1, PC2, and PC3. The composite image was then processed with a High Pass Gaussian filter (Figure 2d) to enhance high-frequency components, effectively suppressing image noise. The resulting output exhibits enhanced linear features, facilitating improved geological interpretation and structural mapping.

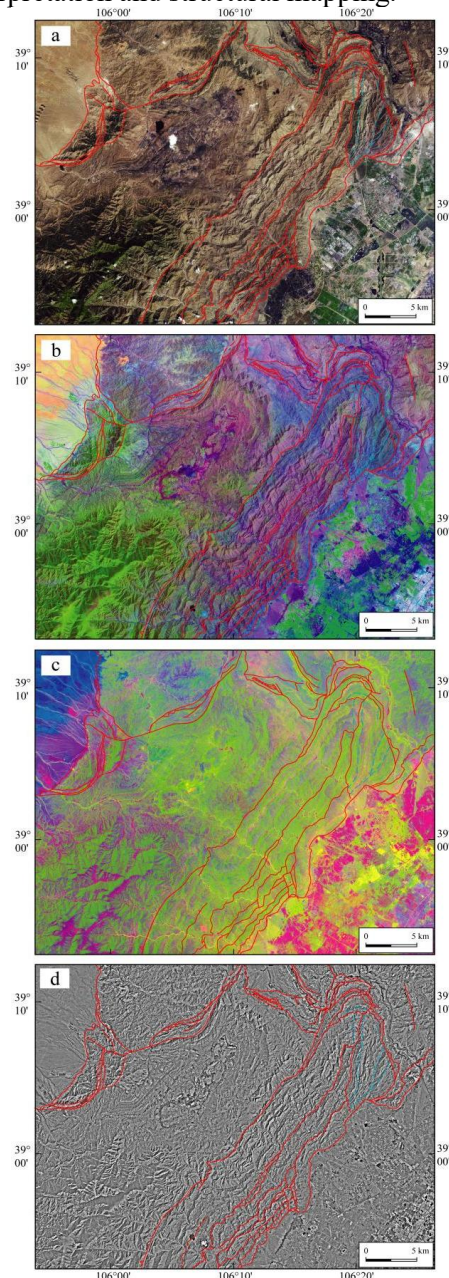


**Figure 2. Remote Sensing Image Processing Results Superimposed Fracture**

a. Google Earth image; b. ETM + images False Color Synthesis results; c. ETM + images Principal Component Analysis results; d. ETM + image Gaussian Filtering enhancement results.

### 3.3 DEM Data Processing

The ASTER GDEM elevation data of the

Shizuishan region were preprocessed in ArcGIS, including coordinate unification, mosaicking, and clipping.

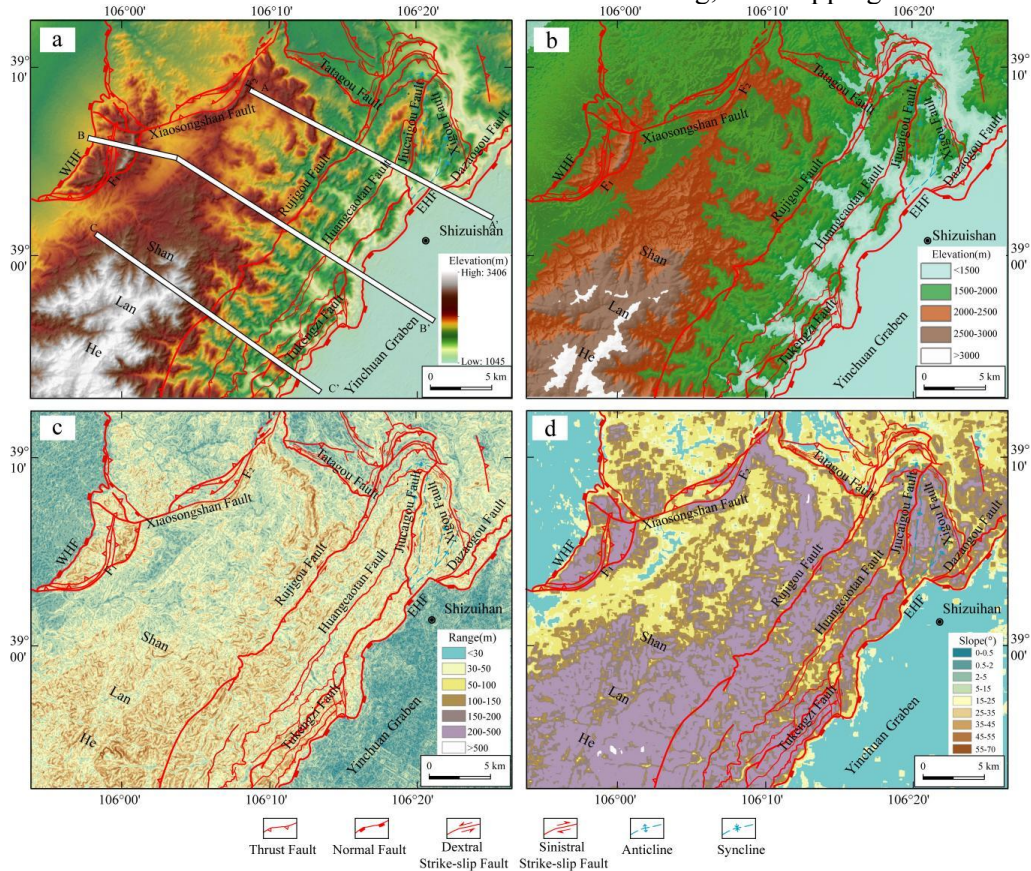


**Figure 3. Regional Aster GDEM Processing Results Superimposed Fracture**

a. Elevation rendering map (Swath profile position); b. Elevation distribution map (modified from [16]); c. Relief amplitude distribution map (modified from [16]); d. Slope distribution map; EHF-Helanshan Eastern Fault; WHF-Helanshan Western Fault.

First, elevation classification and slope factor extraction were conducted, with slope grading performed according to the International Geo-graphical Union's classification standard [20]. Then this paper superimposed the interpreted major linear structures on the DEM maps (Figure 3a, Figure 3b, Figure 3c). Subsequently, focal statistics with a  $15 \times 15$  pixel window were applied to the DEM to extract local maximum and minimum elevations. The relief amplitude map was generated by the difference between the maximum elevation and the minimum elevation through the raster calculator (Figure 3c). Finally, to intuitively analyze the impact of fault activity on regional geomorphology, we set three 500 m wide and 27- 39 km long swath profiles on the digital topographic map. Three NW  $45^\circ$ -oriented profiles (Figure 3a), perpendicular/sub-perpendicular to structural

zones and parallel to ridges, were selected at different locations. Elevation parameters (maximum, minimum, mean, and elevation difference) were calculated at regular intervals [33].

### 4. Tectonic Features

A series of NNE-trending folds and thrust nappe faults developed along the piedmont of the Helanshan, whose kinematic characteristics are crucial for understanding the deformation patterns of orogenic belts. By enhancing the tone and texture of remote sensing images in the study area, we established interpretation markers for faults and fold structures. Based on these markers and combined with field geological phenomena, we identified several linear structures, including the Xiaosongshan thrust nappe fault and the Rujigou thrust fault (Figure 2, Figure 4).

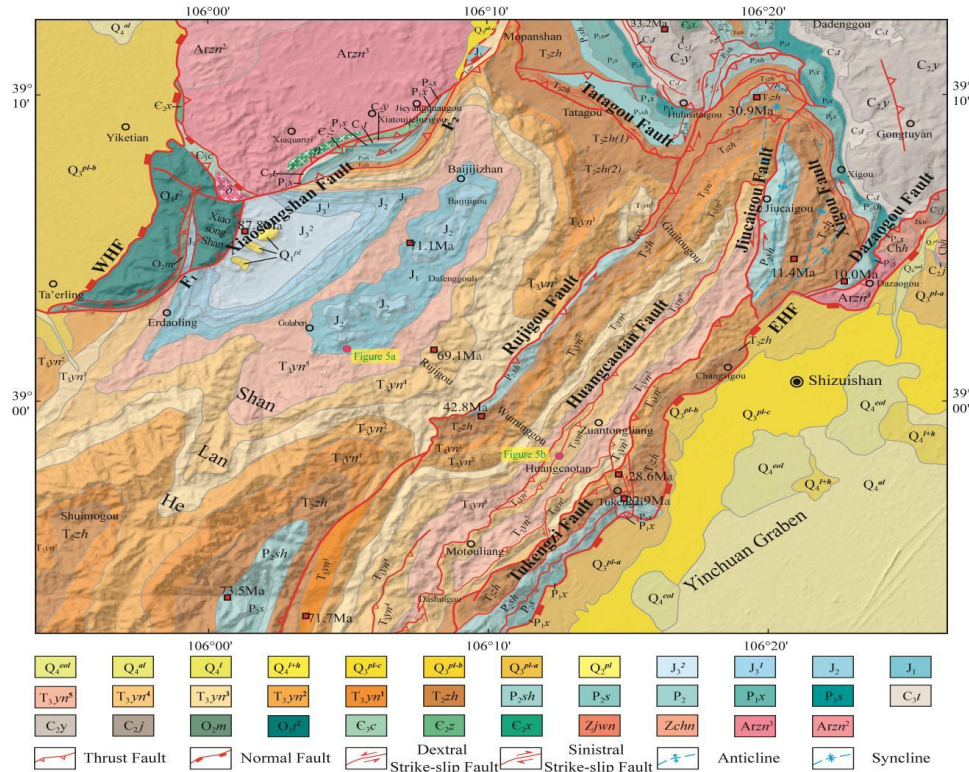


**Figure 4. Shizuishan area in the Middle Segment of Helanshan Tectonic Belt Regional Geological Map (Modified from [15])**

EHF-Helanshan Eastern Fault; WHF-Helanshan Western Fault. AFT ages from [10, 34-35].

Under NW-SE compressive stress, the Ordovician strata in the Xiaosongshan area thrust over Middle Jurassic units (Figure 4, Figure 7), indicating this tectonic event occurred after the Middle Jurassic [24]. In the Gulaben coal mine, the syncline exhibits an NNE trend, with Middle Jurassic (J<sub>2</sub>) gray-green medium-to-thick-bedded coarse-grained graywacke quartz sandstone exposed in its core. The cross-section in Figure 5, located on the southeastern limb of the Gulaben syncline, shows that Lower Jurassic (J<sub>1</sub>) strata developed broad box-shaped anticlines under NW-SE compression. The northeastern limb develops NE-trending imbricate thrust faults F<sub>5</sub> and F<sub>1</sub>, while the southwestern limb contains thrust faults F<sub>2</sub>, F<sub>3</sub>, and F<sub>4</sub>, constituting a local duplex thrust nappe structure style. In the Rujigou-Huangcaotan area, the Upper Triassic Yanchang Formation (T<sub>3yn</sub><sup>4</sup>) developed a series of imbricate thrust faults under NW-SE compression. F<sub>1</sub> and F<sub>2</sub> constitute a duplex structure with floor thrust and passive roof thrust, containing fault-propagation folds, imbricate thrust faults, and local small-scale duplex structures.

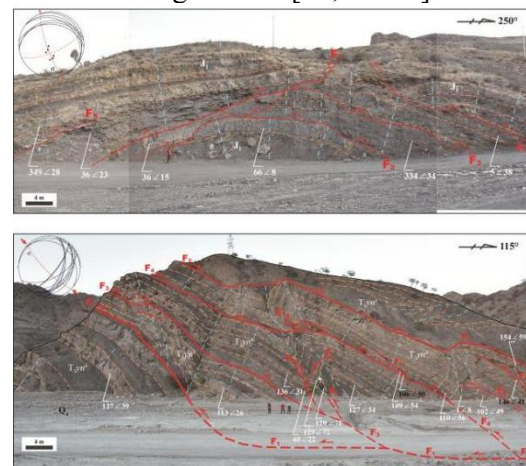


**Figure 5. Field Geological Formations in the Study Area (See Locations in Figure 4)**  
 a. The anticline developed in the J<sub>1</sub>; b. The imbricate thrust faults and fault-related folds are developed in T<sub>3yn</sub> in Huangcaotan area.

**5. Discussion**

The geomorphological characteristics of the Shizuishan-Yinchuan Graben in the middle part of the Helanshan tectonic belt were analyzed by spatial statistical analysis techniques, and the elevation, slope, and degree of relief amplitude were graded and superimposed on the regional faults (Figure 3).

The overall geomorphology of the study area was oriented in a NE-SW direction, with the overall topographic distribution of the west-high and east-low, and the range of elevation was from 1,000 to 3,400 m. Strong tectonic activities are usually manifested by significant differences in topography in terms of elevation, slope, and undulation. The overall topographic relief of the study area gradually decreases along the Helanshan tectonic belt to both sides, and the middle and high-altitude mountain ranges are steeper, and then slows down to the eastern edge of the Yinchuan Graben, presenting topographic and geomorphological features of steep terrain in the west and gradual slopes in the east.

In the Middle Jurassic, the regional tectonic stress field changed, and the nearly north-south compression in the Indosinian period transformed into the nearly east-west compression in the Yanshanian period [8]. The Rujigou tectonic section reflects NW-SE compressional tectonic deformation in the Early Yanshanian (the Middle and Late Jurassic), whereas the Permian strata also developed imbricate thrust structures superimposed on the Indosinian deformation (Figure 7), indicating that the NW-trending contraction occurred after the Middle Jurassic, and chronological data support the regional uplift of the Late Jurassic-Early Cretaceous [23, 34-38].

Combined with the regional elevation information, figures 6 and 7 show that the Xiaosongshan area is a high-elevation region, reaching 2,600 meters. The core of the Tianhua Coal Mine syncline is the Upper Jurassic strata, while the core of the Gulaben Coal Mine Syncline is the Middle Jurassic strata with the absence of Late Jurassic, and the reason for this discrepancy may be the differential denudation after the extrusive orogeny [35].

Since the Early Cretaceous, an extensional tectonic setting was formed in the Helanshan area as a result of the subduction of the Pacific Plate into the Eurasian Plate, and the rift basin began to form, as well as generating a series of boundary normal faults that controlled Cretaceous sedimentation in the Bayanhot Basin and Yinchuan Graben [24, 25, 29, 36]. Apatite fission track ages give a multi-stage differential uplift of the mountain ranges beginning in the Late Cretaceous (71.1 Ma), showing a gradual uplift process from the

center of the Helanshan to the eastern foothills [24-25, 34].

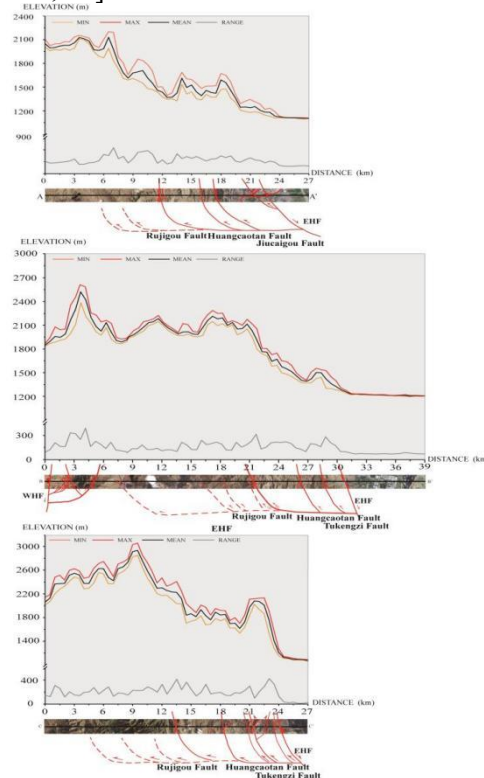


**Figure 6. The Swath Profile Results in the Study Area (See Locations in Figure 3)**

EHF-Helanshan Eastern Fault; WHF-Helanshan Western Fault.

The Cenozoic was an important period for the formation and refinement of the Helanshan-Yinchuan Graben basin-mountain system, and the deep structure of the Ordos Basin periphery shows that upwelling channels of mantle material were formed in the deep Bayanhot Basin and the Yinchuan Graben, which led to the destruction of the Craton lithosphere and contributed to the thinning of the deep lithosphere [12, 27-29, 39-40] (Figure 8). Some scholars have suggested that the early Cenozoic extension of the region is mainly related to the subduction and retreat of the western Pacific plate, while the extension since the late Cenozoic is mainly due to the remote effect of the northeastward spreading of the Tibetan Plateau [30, 40-43]. According to the apatite fission track age gradually transitioned from 71.1 Ma to 11.4 Ma [10, 34-35], this outcome results from the rapid uplift and uplift stripping caused by the fault extensional effect of the Helanshan Eastern Fault, and the stage uplift of the Helanshan in the Oligocene and the Miocene, and the surrounding area experienced subsidence to

form the Yinchuan Graben [34]. After the Oligocene, the basins on the eastern and western sides of the Helanshan subsided more than the Helanshan growth range, resulting in the height difference between the Helanshan

and the Yinchuan Graben as high as 1,300 m (Figure 6, Figure 7), which preserves relatively well-preserved pre-Cenozoic tectonic deformation features in the region.

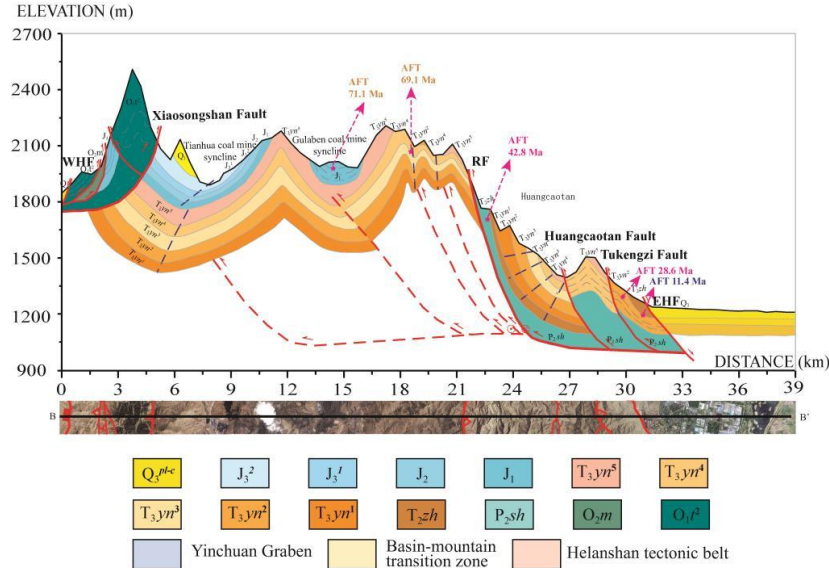


**Figure 7. BB' Swath Profile Corresponds to the Rujigou Tectonic Section (See Locations in Figure3).**

EHF-Helanshan Eastern Fault; WHF-Helanshan Western Fault; AFT ages from [10, 34-35]

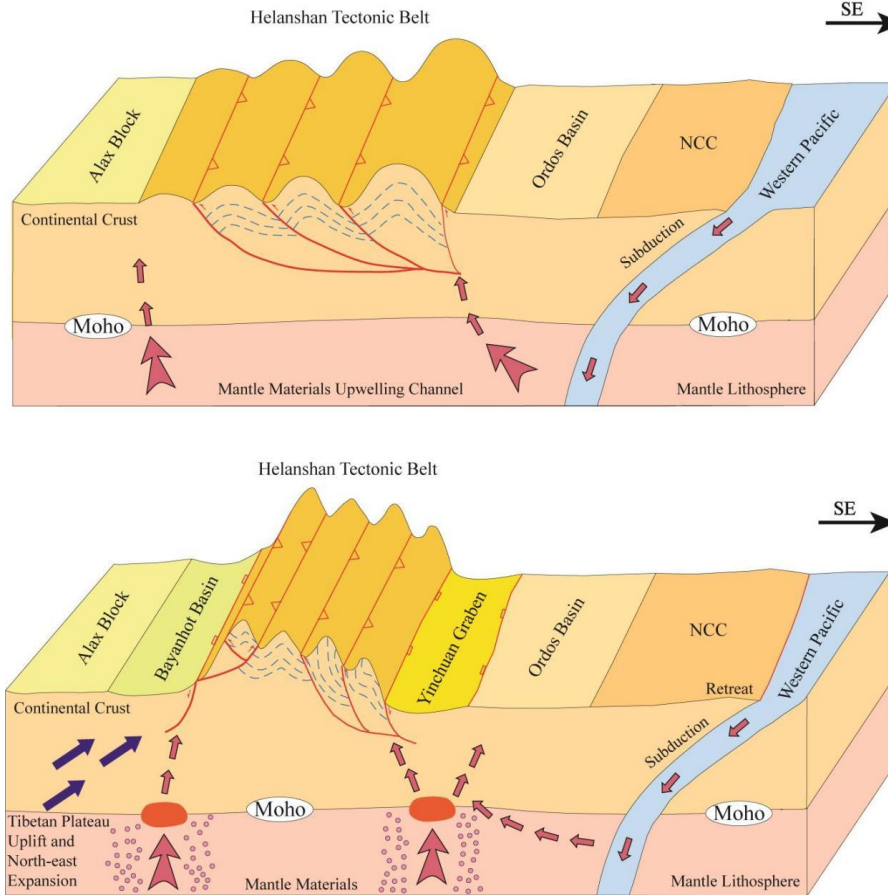


**Figure 8. Evolution Model of Helanshan Tectonic Belt (Modified from [12]).**

## 6. Conclusion

This paper comprehensively analyzes the regional tectonic and geomorphological features and regional tectonic evolution of the study area through the ETM+ images and DEM data of the Shizuishan area, combined with the deformation in the field. The results reveal that the Helanshan region experienced intense intracontinental compressional deformation due to the Yanshanian Orogeny, forming NNE-SSW-trending imbricated thrust-nappe structures, with the mountain uplift manifesting as low elevations in the west and high elevations in the east. From the Oligocene to Miocene, influenced by the north-eastward expansion of the Tibetan Plateau and the subduction and retreat of the Western Pacific Ocean, the Helanshan Eastern Fault reversed, causing in the tectonic subsidence of the Yinchuan Graben and the periodic uplift of the Helanshan, resulting in a geomorphological pattern that is higher in the west and lower in the east.

## Acknowledgments

This paper is supported by the China National Science and Technology Major Project (No. 2024ZD1001100) and the China Geological Survey (No. DD20242780). We thank the reviewers and editors for valuable revisions to the article, and the National Aeronautics and Space Administration (NASA) and Geospatial Data Cloud for providing Landsat 7 ETM+ image and ASTER DEM data.

## References

- [1] J. Liu, J. Y. Zhang, Y. K. Ge, et al. Tectonic Geomorphology: An Interdisciplinary Study of the Interaction among Tectonic Climatic and Surface Processes. *Chinese Science Bulletin*, 2018, 63(30): 3070-3088. (in Chinese)
- [2] S. Wang. *Geology and Geomorphology (The Third Edition)*. Beijing: China Agricultural University Press, 2022: 1-396. (in Chinese)
- [3] P. J. Cao, S. Y. Cheng, H. X. Lin, et al. DEM in Quantitative Analysis of Structural Geomorphology: Application and Prospect. *Journal of Geomechanics*, 2021, 27(6): 949-962. (in Chinese)
- [4] Y. Dai, X. Y. Wang, S. L. Wang, et al. The Geomorphological Index Reflects the Neotectonic Activity in the Wenchuan River Basin of Northeastern Tibet Plateau. *Acta Geographica Sinica*, 2016, 71(3): 412-421. (in Chinese)
- [5] L. Polidori and M. E. Hage. Digital Elevation Model Quality Assessment Methods: A Critical Review. *Remote Sensing*, 2020, 12(21): 3522.
- [6] M. Wang, J. F. Li, X. L. Wang. *Regional Geology of China-Ningxia*. Beijing: Geological Publishing House, 2017: 1-45. (in Chinese)
- [7] X. H. Chen, S. W. Dong, W. Shi, et al. Construction of the Continental Asia in Phanerozoic: A Review. *Acta Geologica Sinica - English Edition*, 2022, 96(1): 26-51.
- [8] S. W. Dong, Y. Q. Zhang, C. X. Long, et al. Jurassic Tectonic Revolution in China and New Interpretation of the "Yanshan Movement". *Acta Geologica Sinica - English Edition*, 2008, 82(2): 334-347.
- [9] X. H. Chen, J. Y. Li, S. W. Dong, et al. Jurassic Tectonic Deformation of the Ningwu-Jingling Basin in Central North China Craton and the Initiation of the Yanshanian Orogenic Event. *Geotectonica et Metallogenia*, 2019, 43(3): 389-408. (in Chinese)
- [10] G. Z. Shi, C. B. Shen, M. Zattin, et al. Late Cretaceous-Cenozoic Exhumation of the Helanshan Mt Range, Western Ordos Fold-thrust Belt, China: Insights from Structural and Apatite Fission Track Analyses. *Journal of Asian Earth Sciences*, 2019, 176: 196-208.
- [11] C. H. Liu, F. He, Z. Y. Li, et al. Transformation of Basin-mountain Structure and the Tectonic-sedimentary Response in the Southwestern Ordos Basin in Late Mesozoic to Cenozoic. *Uranium Geology*, 2023, 39(6): 875-891. (in Chinese)
- [12] D. X. Xu, Z. G. Shao, X. H. Chen, et al. Deep Electrical Structure and Dynamic Mechanism of the Helanshan Tectonic Belt. *Geological Bulletin of China*, 2024, 43(11): 1921-1936. (in Chinese)
- [13] X. Y. Yang, Y. P. Dong. Multiple Phases of Deformation in the Southern Helanshan Tectonic Belt, Northern China. *Journal of Asian Earth Sciences*, 2020, 201: 104497.
- [14] Z. P. Zhou, X. H. Chen, Z. G. Shao, et al. Differential Deformation Mechanism of

- E-W-trending Weiningbeishan Fold-thrust Belt from Central Ningxia, NW China. *Geological Journal*, 2024, 59(6): 1841-1860.
- [15] D. X. Xu, Z. G. Shao, X. H. Chen, et al. Triassic Contractional Deformation and Sedimentary Response in the Helanshan Fold-thrust Belt, Northwest China: Evidence from Growth Strata. *International Geology Review*, 2025: 1-23.
- [16] X. R. Yang, M. K. Sheng, W. C. Ding, et al. Analysis of tectonic geomorphological characteristics based on DEM: a case study of Shizuishan, China. *Third International Conference on Geographic Information and Remote Sensing Technology (GIRST 2024)*, 135510C.
- [17] K. Amri, G. Rabai, I. M. Benbakhti, et al. Mapping Geology in Djelfa District (Saharan Atlas, Algeria), Using Landsat 7 ETM+ Data: an Alternative Method to Discern Lithology and Structural Elements. *Arabian Journal of Geosciences*, 2017, 10(4): 87.
- [18] L. L. Han, W. C. Ding, X. H. Chen, et al. Linear Structure Extraction and Quantitative Analysis of Multi-source Remote Sensing Information in West Junggar Basin. *Geology in China*, 2019, 46(5): 1209-1223. (in Chinese)
- [19] W. C. Ding, T. D. Li, X. H. Chen, et al. Intra-continental Deformation and Tectonic Evolution of the West Junggar Orogenic Belt, Central Asia: Evidence from Remote Sensing and Structural Geological Analyses. *Geoscience Frontiers*, 2020, 11(2): 651-663.
- [20] Z. C. Cao, L. D. Zhu, W. G. Yang, et al. Tectonic Geomorphological Analysis of Yadong-Gulu and Cona-Oiga Rift System Based on ASTER-GDEM Data. *Science Technology and Engineering*, 2022, 22(25): 10896-10905. (in Chinese)
- [21] D. X. Xu, B. Yang, Z. G. Shao, et al. A Hyperspectral Analysis of Alteration Zoning in the Hadamengou Gold Deposit and its Significance for Ore Prospecting. *Remote Sensing for Natural Resources*, 2023, 35(1): 123-131. (in Chinese)
- [22] S. Y. Hong, X. H. Shen, F. Jing, et al. Tectonic and Geomorphological Characteristics of Altai Mountains Based on SRTM-DEM. *Remote Sensing for Land AND Resources*, 2007, 3: 62-66. (in Chinese)
- [23] X. F. Huang, W. Shi, P. Chen, et al. Superposed Deformation in the Helanshan Structural Belt: Implications for Mesozoic Intracontinental Deformation of the North China Plate. *Journal of Asian Earth Sciences*, 2015, 114: 140-154.
- [24] X. Y. Yang, Y. P. Dong. Mesozoic and Cenozoic Multiple Deformations in the Helanshan Tectonic Belt, Northern China. *Gondwana Research*, 2018, 60: 34-53.
- [25] Z. Q. Liu. Basin-mountain conversion of Yinchuan Basin and its Coupling Relation to Helan Mountain. *Journal of Hefei University of Technology (Natural Science)*, 2014, 37(11): 1366-1371. (in Chinese)
- [26] S. Y. Feng, R. Gao, C. X. Long, et al. The Compressive Stress Field of Yinchuan Graben: Deep Seismic Reflection Profile. *Chinese Journal of Geophysics*, 2011, 54(3): 692-697. (in Chinese)
- [27] B. J. Liu, S. Y. Feng, J. F. Ji, et al. Lithospheric Structure and Faulting Characteristics of the Helan Mountains and Yinchuan Basin: Results of Deep Seismic Reflection Profiling. *Science China Earth Sciences*, 2017, 47(2): 179-190. (in Chinese)
- [28] X. Li, Y. Chen, X. B. Tian, et al. Magnetotelluric Evidence for Distributed Lithospheric Modification Beneath the Yinchuan-Jilantai Rift System and Its Implications for Late Cenozoic Rifting in Western North China. *Journal of Geophysical Research: Solid Earth*, 2022, 127(3): e2021JB022585.
- [29] X. F. Huang, S. Y. Feng, R. Gao, et al. High-resolution Crustal Structure of the Yinchuan Basin Revealed by Deep Seismic Reflection Profiling: Implications for Deep Processes of Basin. *Earthquake Science*, 2016, 29(2): 83-92.
- [30] W. Shi, S. W. Dong, J. Hu. Neotectonics around the Ordos Block, North China: A Review and New Insights. *Earth-Science Reviews*, 2020, 200(5): 102969.
- [31] M. Li, W. H. Li, H. G. Zhao, et al. Sedimentary Characteristics and Geological Significance of Triassic in the Helan Mountains. *Journal of northwest university (natural science edition)*, 2019, 49(5): 745-754. (in Chinese)
- [32] G. S. Zhao, Y. Du, F. Ling, et al. Analysis

- of Influencing Factors of Elevation Difference between ASTER GDEM and SRTM3. *Science of Surveying and Mapping*, 2012, 37(4): 167-170. (in Chinese)
- [33] B. W. Zhou, W. F. Ma, Y. Long, et al. Application of Swath Profile Extraction Method Based on ArcGIS in Geomorphology Analysis. *Geography and Geo-Information Science*, 2011, 27(3): 42-44. (in Chinese)
- [34] J. H. Liu, P. Z. Zhang, D. W. Zheng, et al. Stripping Characteristics and Uplift Model of Late Cenozoic Uplift in Helan Mountain. *Science in China*, 2010, 40(1): 50-60. (in Chinese)
- [35] H. G. Zhao, C. Y. Liu, F. Wang, et al. Time Limit and Evolution of Helan Mountain Uplift. *Science in China Press*, 2007, 37 (S1): 185-192. (in Chinese)
- [36] X. B. Hou, H. Z. Cui and Y. L. Xun. Analysis of Structural Styles and Formation and Evolution of Different Tectonic Layers in Yinchuan Basin. *Journal of Northeast Petroleum University*, 2012, 36(6): 28-33. (in Chinese)
- [37] J. Zhang, J. Y. Li, Y. F. Li, et al. Mesozoic-Cenozoic Multi-Stage Intraplate Deformation Events in the Langshan Region and their Tectonic Implications. *Acta Geologica Sinica*, 2014, 88(1): 78-102.
- [38] J. H. Ma, D. F. He, B. Z. Kai, et al. Stratigraphic sequence and tectonic evolution of Helan Mountain tectonic belt *Acta Petrologica Sinica*, 2019, 35(4): 1121-1142. (in Chinese)
- [39] G. J. Wu, H. B. Tan, K. Sun, et al. Characteristics and Tectonic Significance of Gravity Anomalies in the Helanshan-Yinchuan Graben and Adjacent Areas. *Chinese Journal of Geophysics*, 2020, 63(03): 1002-1013. (in Chinese)
- [40] L. Q. Zhao, X. Y. Sun, Y. Zhan et al. Characteristics of the Three-dimensional Deep Electrical Structure in the Helan Mountains-Yinchuan Basin and Its Geodynamic Implementations. *Science China Earth Sciences*, 2023, 53(03): 481-496. (in Chinese)
- [41] G. Z. Shi, C. J. Soares, C. B. Shen, et al. Combined Detrital Zircon Fission Track and U-Pb Dating of the Late Paleozoic to Early Mesozoic Sandstones in the Helanshan, Western Ordos Fold-thrust Belt: Constraints for Provenance and Exhumation History. *Journal of Geodynamics*, 2019, 130: 57-71.
- [42] X. B. Liu, J. M. Hu, W. Shi, et al. Palaeogene-Neogene Sedimentary and Tectonic Evolution of the Yinchuan Basin, Western North China Craton. *International Geology Review*, 2020, 62(1): 53-71.
- [43] P. Su, H. He, X. Tan, et al. Initiation and Evolution of the Shanxi Rift System in North China: Evidence from Low-temperature Thermochronology in a Plate Reconstruction Framework. *Tectonics*, 2021, 40, e2020TC006298.